Analytical Methods

Analytical Methods

www.rsc.org/methods

ROYAL SOCIETY OF CHEMISTRY

ROYAL SOCIETY OF CHEMISTRY

www.rsc.org/methods

190x142mm (300 x 300 DPI)

Repeatability and reproducibility of desorption electrospray ionization-mass spectrometry (DESI-MS) for the imaging analysis of human cancer tissue: a gateway for clinical applications

Nima Abbassi-Ghadi[1‡] & Emrys A. Jones[1‡], Kirill A. Veselkov[1], Juzheng Huang[1], Sacheen Kumar[1], Nicole Strittmatter[1], Ottmar Golf[1], Hiromi Kudo[2], Robert D Goldin[2], George B Hanna[1], Zoltan Takats[1]*

[1]Department of Surgery and Cancer, Imperial College London, 10th Floor QEQM Wing, St Mary's Hospital, London, UK, W2 1NY

[2]Centre for Pathology, Imperial College London, 4th Floor Clarence Wing, St Mary's Hospital, London, UK, W2 1NY

1 **Abstract**

2 In this study, we aim to demonstrate the repeatability and reproducibility of DESI-MS for the

3 imaging analysis of human cancer tissue using a set of optimal geometric and electrospray

4 solvent parameters. Oesophageal cancer tissue was retrieved from four quadrants of a freshly

5 removed tumor specimen, snap frozen, cryo-sectioned and mounted on glass slides for DESI-MS

6 image acquisition. Prior to assessing precision, optimal geometric and electrospray solvent

7 parameters were determined to maximize the number of detected lipid species and associated

8 Total Ion Count (TIC). The same settings were utilized for all subsequent experiments.

9 Repeatability measurements were performed using the same instrument, by the same operator on

10 a total of 16 tissue sections (four from each quadrant of the tumor). Reproducibility

11 measurements were determined in a different laboratory, on a separate DESI-MS platform and

12 by an independent operator on 4 sections of one quadrant and compared to the corresponding

13 measurements made for the repeatability experiments. The mean±SD CV of lipid ion intensities

14 was found to be 22±7% and 18±8% as measures of repeatability and reproducibility,

15 respectively. In conclusion, DESI-MS has acceptable levels of reproducibility for the analysis of

16 lipids in human cancer tissue and is suitable for the purposes of clinical research and diagnostics.

17

18

19

20

21

22   **Introduction**

23   Mass spectrometry imaging (MSI) can be used for spatially resolved analysis of ionised

24   metabolites from biological tissue sections. The chemical information is often represented in the

25   form of false colour images, that help the analyst to obtain metabolic profiles from histologically

26   distinct areas, rather than extracting non-specific metabolites from blocks of heterogeneous

27   tissue as is performed in analytical protocols involving tissue homogenization. Matrix assisted

28   laser desorption ionization mass spectrometry (MALDI-MS), secondary ion mass spectrometry

29   (SIMS) and desorption electrospray ionization mass spectrometry (DESI-MS) are common MSI

30   techniques that have been used to investigate a range of diseases including cancer, neurological

31   disorders and atherosclerosis.[1-10]

32   DESI-MS is particularly suited at for the detection of lipids in biological tissue,[9-11] which are

33   defined as hydrophobic or amphiphilic low molecular weight molecules that originate mostly

34   from biological membranes.[12] Alterations in lipid metabolism in the cancer disease state has

35   attracted significant scientific interest and has bolstered the new discipline of lipidomics, which

36   is defined as the emerging field of systems-level analysis of lipids and factors that interact with

37   lipids.[13]

38   In case of DESI-MS analysis, a pneumatically assisted electrospray comprising high-velocity

39   charged liquid micro-droplets, molecular clusters and gaseous ions is directed at a surface. On

40   the impact of micro-droplets, the surface is wetted and the solvent extracts analyte molecules

41   into the liquid film temporarily present on the surface. The impact of incoming droplets results in

42   the formation of secondary droplets departing from the surface. Given that the surface is

43   electrically non-conductive, the secondary droplets will still carry net electric charge. Since the

3

44 droplets already contain species dissolved from the surface, these species may undergo an

45 electrospray-like ionization mechanism. The effective formation of gaseous ions usually takes

46 place in the atmospheric interface of the mass spectrometer (MS).[14] Due to their high abundance,

47 limited solubility in aqueous solvent systems and the virtually zero desorption enthalpy (i.e. from

48 the surface of electrically charged droplets) of ionization, lipids species are the dominant bio-

49 molecular compound class detected by DESI-MS (and any other electrospray-like ionization

50 methods). The ionization involves minimal fragmentation of the molecules, which improves the

51 specificity of lipid identification in complex biological mixtures. Identification performance can

52 be further enhanced by the application of high resolution/tandem mass spectrometry.

53 There have been questions regarding the analytical performance characteristics of DESI-MS

54 including ion suppression effects (i.e. the degree that analytes suppress the ionization of other

55 analytes present in the same sample) and overall yields (i.e. the fraction of the original material

56 that is converted into gas-phase ions at the detector of the MS).[14] Furthermore, fluctuations in the

57 solvent composition/voltage, gas flow rate, solvent flow rate and geometric set-up can also cause

58 variation within the obtained mass spectral datasets.[15-19] Bias introduced by these factors may

59 compromise the precision of the technique and as a consequence may hinder the translation of

60 the technique to the level of routine clinical applications. The U.S. Food and Drug Agency

61 (FDA) states that the co-efficient of variance (CV) of reproducibility should not exceed 20% for

62 analytical techniques.[20]

63 In this study, we aim to demonstrate that by using a set of optimized geometric and electrospray

64 parameters DESI-MS is capable of yielding highly repeatable spectral profiles of human cancer

65 tissue on the same instrument and reproducible measurements performed by an independent

66 operator using a different instrumental setup in a different laboratory.

67 **Experimental section**

68 **Samples**

69 Specimen retrieval and analysis was performed under an approved and institutional review board

70 protocol, with informed written consent obtained by a licensed clinician. Tumor tissue obtained

71 from a patient with oesophageal adenocarcinoma was chosen as the measurand for comparative

72 analysis. In order to reduce biological variability affecting our measurements, we chose a

73 macro/microscopically homogenous tumor with uniform histological characteristics. Samples

74 were taken from each quadrant of the tumour after surgical resection of the oesophagus. The four

75 tissue samples were stored at -80°C prior to cryo-sectioning at 15μm thickness using a Bright

76 5030 Cryotome (Bright Instruments, Cambridgeshire, UK) set at -20°C, and thaw mounted onto

77 SuperFrost$^®$ Plus Glass slides (Thermo Fisher Scientific Inc., USA). The slides were stored in

78 closed containers at -80°C and were allowed to thaw under nitrogen flow at room temperature for

79 a standardized five minutes prior to DESI-MS analysis.

80

81 **Instrumentation**

82 DESI-MS analysis was performed using an Exactive Fourier-transform Orbitrap mass

83 spectrometer (Thermo Fisher Scientific Inc., Bremen, Germany) controlled by XCalibur 2.1

84 software and operated in negative ion mode. Data was acquired at a nominal mass resolution of

85 100,000 FWHM (mass accuracy of <4ppm); injection time was set to 1000 ms; mass to charge

86 (*m/z)* range was 150–1,000; capillary temperature was set to 250°C; capillary voltage was 50V;

87 tube lens voltage was -150V; and skimmer voltage was -40V. The MS parameters were kept

88 constant for the purpose of DESI-MS sprayer optimization. A 1/16" Swagelok T element-based

89 DESI-MS sprayer (for the details of the set-up see supplementary file 1) was used in conjunction

90 with a home built 3D XYZ integrated linear stage, which acts as a sample holder and positioning

91 device for the sprayer relative to the MS capillary inlet and sample (for set-up see supplementary

92 file 2).

93
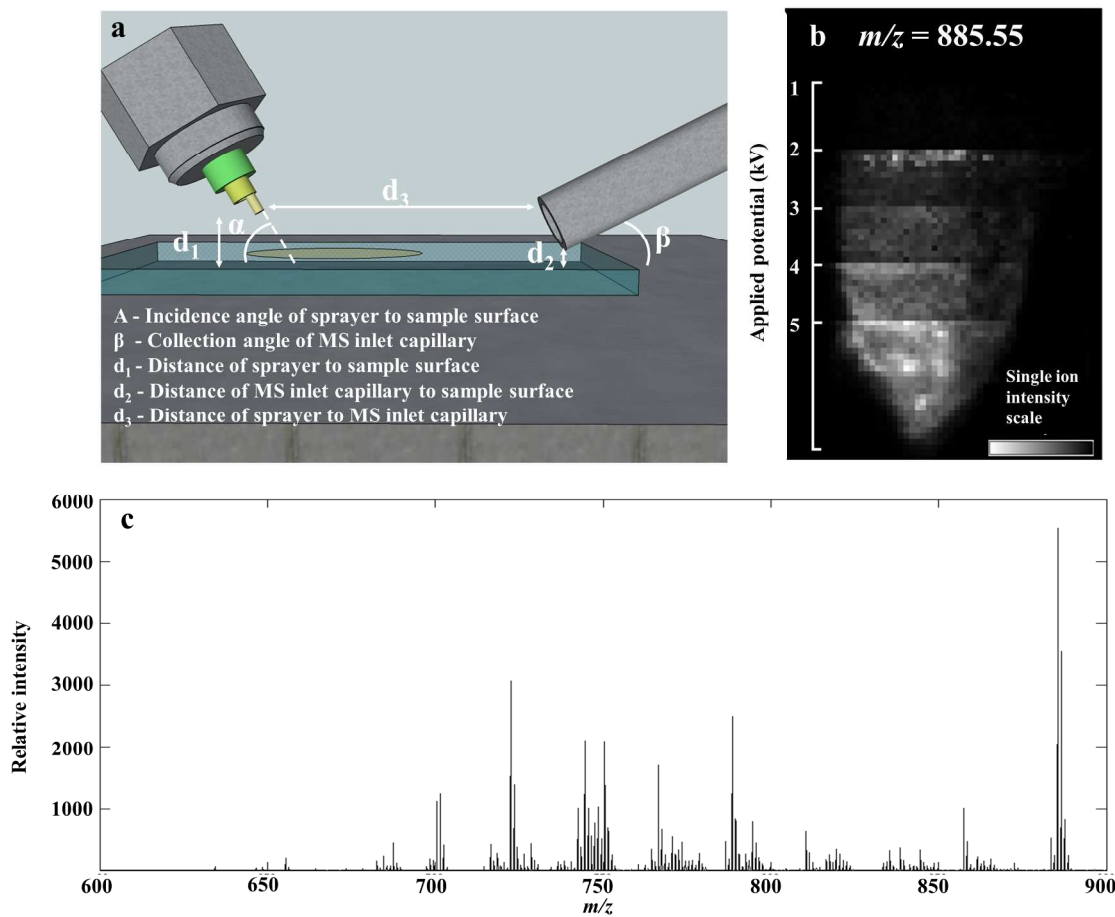
94 ***Figure 1*** *Optimization methodology **a)** Illustration of the DESI-MS sprayer and mass*
95 *spectrometer (MS) inlet with respect to geometrical parameters **b)** An example of the*
96 *optimization experiment: the settings of a given variable, in this case electric potential applied to*
97 *generate the electrospray, is changed at fixed intervals during an imaging experiment on a*
98 *single tissue section **c)** representative median mass spectrum in the 600-900 m/z range for the*
99 *tissue analysed in this study.*

100

101

Process of Optimization

104 We optimized the parameters of the DESI-MS set-up for the purpose of lipidomic profiling by

105 determining optimal settings for maximum ion yield of lipid species. Geometric parameters of

106 the DESI-MS sprayer and electrospray solvent parameters were adjusted in a systematic fashion

107 to determine the optimum settings. Geometric parameters included the height of sprayer tip

108 relative to the sample surface, distance of sprayer tip from the MS inlet capillary and the angle of

109 the sprayer tip to the sample surface (figure 1a). Electrospray solvent parameters included the

110 ratio of MeOH and H_2O in the solvent, solvent flow rate, nebulizing gas flow rate, and electric

111 potential applied to generate the electrospray.

112 Distances were manually adjusted on the DESI-MS sprayer mount using built-in micrometre

113 screw gauges providing accuracy down to 50μm. The angle of the sprayer was manually adjusted

114 with a rotational manipulator with an accuracy of 1 degree. Solvent flow rates were adjusted with

115 a Sunchrom Micro Syringe pump carrying a 200μl syringe. Gas pressure was set using a BOC

116 Series 8500 nitrogen regulator, with an accuracy of 0.5 bar.

117 Multiple settings of each variable were tested on separate single tissue sections (example, Figure

118 1b). The tissue sections used for the optimization experiments were all from the same sample

119 from the first quadrant of the tumor, thereby minimizing biological variability influencing the

120 results. When adjusting the settings of one variable, all other variables were kept at pre-

121 determined values as follows: 2mm distance from sprayer tip to sample surface, 14mm from

122 sprayer tip to MS capillary inlet, 80° incidence angle of sprayer to surface, 95:5 v/v MeOH: H_2O

123 solvent concentration, 1.5μl/min solvent flow rate, 4 bar gas inlet pressure and a spray voltage of

124 4.5kV. The MS inlet capillary had a collection angle of 10° and set at 500μm from the sample

7

125 surface and was not adjusted for optimization. The lateral resolution of the data acquisition (pixel

126 size) was also kept constant at 75μm. Due to the inter-dependence of the solvent flow rate and

127 gas inlet pressure for generating the nebulized solvent; these variables were tested together

128 through multiple combinations of their settings.

129 **Determination of precision**

130 The precision of an instrument is defined as the closeness of agreement between independent test

131 results obtained under stipulated conditions.[21] Quantitative measures of precision depend

132 critically on these conditions. Repeatability and reproducibility conditions are particular sets of

133 extreme stipulated conditions. Repeatability is the precision obtained under the same conditions

134 when independent test results are obtained with the same method, on identical test items, in the

135 same laboratory, by the same operator, using the same equipment, and within short intervals of

136 time. Repeatability leads to an estimate of the minimum value of precision. Reproducibility is the

137 precision obtained under changing conditions when independent test results are obtained with the

138 same method, on identical test items, but in different laboratories, with different operators, using

139 different (or recalibrated) equipment.

140

141 A total of 16 tissue sections including four from each quadrant of the tumor were subjected to

142 DESI-MS image acquisition in a random order, performed consecutively in a single time frame,

143 in the same laboratory and by the same operator for measures of repeatability. All geometric and

144 electrospray parameters were kept constant as per the optimized values.

145

146 A total of 4 tissue sections from a single quadrant of the tumor were subjected to DESI-MS

147 image acquisition in a random order, performed consecutively, in a different laboratory, with a

148 different operator, using a different sprayer and MS (LTQ Orbitrap Discovery, Thermo Fisher

149 Scientific Inc., Bremen, Germany) and compared to the initial data set of the same quadrant, for

150 measures of reproducibility. All geometric, electric and solvent parameters of the DESI-MS

151 source were kept constant as per the previously determined optimized values. Stored samples of

152 the tissue sections were analysed in the same time frame as the repeatability experiments to

153 avoid any bias introduced through storage.

154 **Data analysis methods**

155 Following DESI-MS image acquisition, an imzML converter (Justus-Liebig-Universität,

156 Giessen, Germany) was used to combine the series of raw files for each imaging dataset. The

157 subsequent imzML files were then read into a MATLAB (MathWorks) environment using an in-

158 house written function, incorporating a mass range selection of m/z 600 to 900 to limit spectral

159 feature identification to lipids.

160 *Optimization*

161 The ion images from the tissue sections used for optimization were divided into sub-segments,

162 directly relating to each setting or combination of settings of the variables under investigation

163 (figure 1b). The relevant mass spectra (approximately 300) from each sub-segment were then

164 extracted from the corresponding image dataset and a median spectrum was calculated. The

165 number of spectral features, defined as the quantity of mass spectral peaks between the m/z range

166 600-900 and with a height filter set to ten times the baseline noise, was calculated for each

167 median spectrum using the *mspeaks* function within the bioinformatics toolbox of MATLAB.

168 The spectral features were not de-isotoped for the purpose of the optimisation data analysis. The

169 total ion count (TIC) was then calculated for the defined spectral features for each median

170 spectrum.

171 *Repeatability*

172 A full resolution median spectrum was created from the tumour specific regions of the 16

173 imaging dataset, in order to remove isotope peaks such that they were not included in the

174 comparison. Following identification of all peaks in the 600-900 Da mass range, an in-house

175 written de-isotoping algorithm scanned the surrounding of every peak for its carbon-13 isotope.

176 A peak was identified as an isotope peak if 1) the mass to charge ratio difference to its parent

177 peak was (1.0034/abs (z) ± tolerance) and 2) the intensity difference matched theoretical value ±

178 tolerance. Approximate theoretical carbon-13 intensities were determined by using a virtual

179 lipid, 'averagine', based on the elemental composition of 21 representative lipid species. Peaks

180 not having a 13C isotope peak and all found isotope peaks were excluded from the 16 imaging

181 datasets. In order to ensure sufficient intensity for a meaningful comparison over all datasets,

182 peaks with intensity less than ten times the base noise level in the median spectrum were

183 removed, this resulted in a total of 65 lipid peaks for comparative analysis (supplementary file

184 3). Integration regions of ±50 ppm were set for peak extraction from the median fold normalised

185 spectra with the data then stored in a sixteen-member data structure, with each cell containing the

186 65 extracted lipid peaks for each individual spectrum from the sixteen datasets.

187 For the CV calculations, 10 spectra were randomly selected from either a single sample (intra-

188 section), or samples from the same quadrant (intra-quadrant) or samples from the whole dataset

189 (inter-quadrant) and averaged to create a single data vector. For each data vector, the 65 pre-

190   determined peak regions were integrated and the mean of their CVs were calculated. This

191   process was repeated 50 times for each sampling group. The mean and standard of deviation of

192   the 50 mean CVs of each sample group were calculated.

193   In order to compare the lipid profiles of the 16 tissue sections, the average of 10 full spectra (m/z

194   600-900), repeated 25 times were randomly collected from each of the 16 imaging datasets, pre-

195   processed (vide supra), log transformed, and analysed by principal component analysis (PCA).

196   Further comparisons were made by hierarchical cluster analysis (HCA). In this case, four regions

197   of interest were manually selected from each of the 16 ion images and their corresponding

198   spectral data were averaged, giving a total of 64 data vectors. Pairwise distances were calculated

199   with the 'correlation' metric within the *pdist* MATLAB function. The hierarchical tree was

200   encoded using the 'average' metric for the *linkage* function.

201   The correlation pairwise distance metric calculates the distances based on one minus the

202   correlation between points, whilst the average metric for computing distance between clusters

203   uses the un-weighted average distance. These metrics were selected as they gave the highest

204   score from all available combinations for a cophenetic correlation calculation (obtained using the

205   *cophenet* function). This is a measure of correlation between the distances obtained from the tree

206   and those used to construct the tree; a higher correlation score indicates a more faithful

207   representation of the original distances.

208   ***Reproducibility***

209   Data from the eight tissue sections (four from each instrument) were pre-processed (as per the

210   repeatability analysis). Due to the higher sensitivity of the Exactive instrument, not all of the

211   peaks from the first analysis were consistently detected within the LTQ Orbitrap data. Using the

11

212   same conservative ten times baseline noise metric as previously, the peak list for the comparison

213   was reduced to 27 lipid species. The CV was calculated for their ion intensities across the four

214   tissue sections for each separate instrument followed by combination of the whole data set.

215

Results and Discussion

216   **Results and Discussion**

217   **Optimization of experimental parameters**

218   The number of spectral features in the *m/z* range of 600-900 and their associated TIC values

219   obtained for various settings of geometric and electrospray parameters are demonstrated in figure

220   2. Previous studies investigating the droplet dynamics of DESI-MS support our findings

221   regarding the optimum values for different parameters.[14-18,23-29]

222   The optimal settings determined for our DESI-MS ion source were a sprayer to surface distance

223   of 2mm, sprayer to MS capillary inlet of 14mm, solvent flow rate of 1.5ul/min, gas flow rate of 7

224   bars, 90:10 v/v MeOH: H_2O solvent concentration and a spray potential of 5kV. An incidence

225   angle of 75 degrees was selected due to the minimal variation observed in the studied range of

226   values. We compared the outcome of two adjacent sections using the new versus our preliminary

227   set of experimental values and demonstrated a 192% increase in the number of detected spectral

228   features and increase in TIC by one order of magnitude in the 600-900 m/z range (figure 2h).

229

12
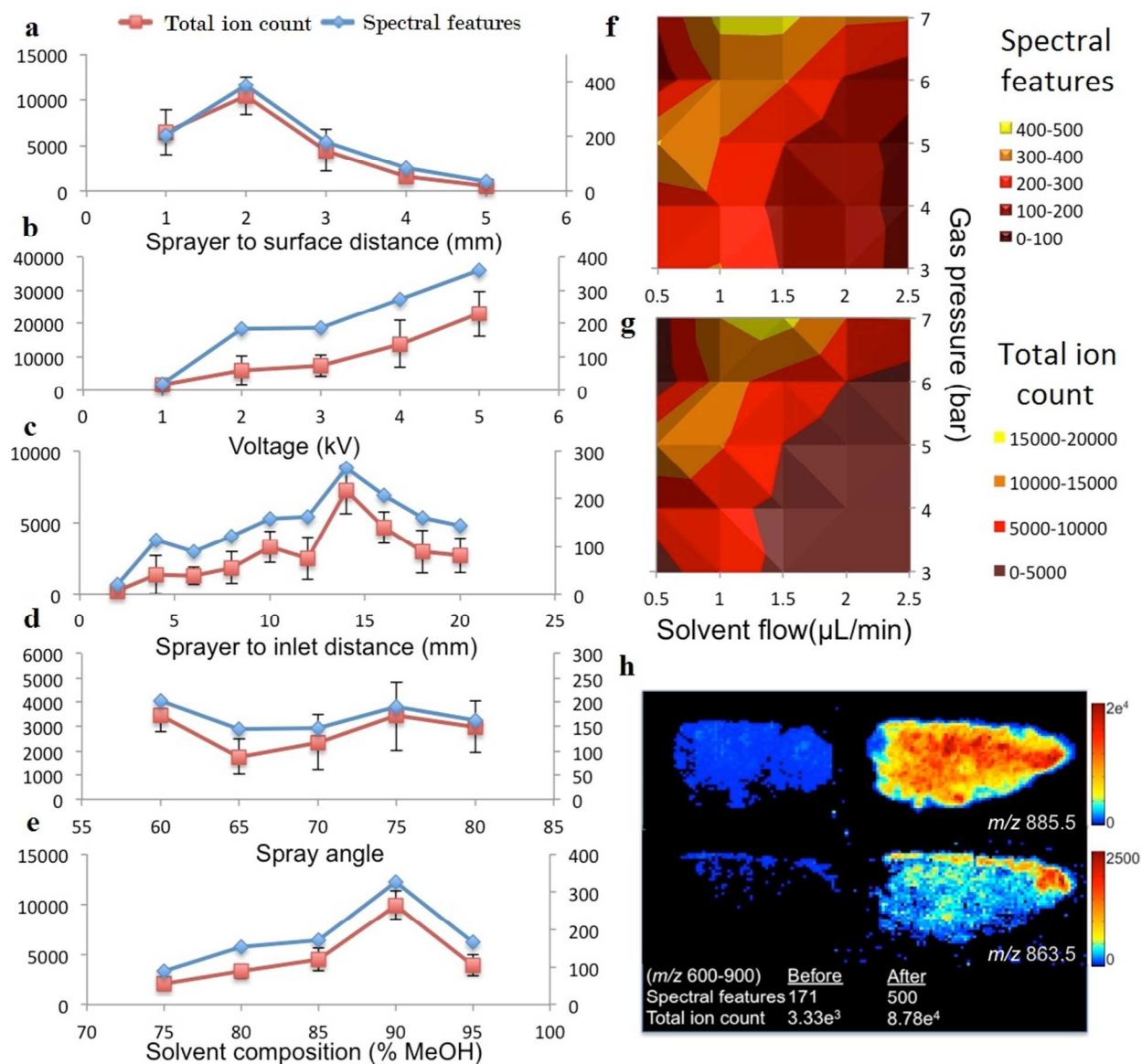
Figure 2 a-e) *effect of different variable settings on total ion count (red) and spectral features (blue) for the m/z 600-900 spectral region, error bars indicate 95% confidence intervals **f)& g)** surface maps of spectral features and total ion count for the inter-relationship between solvent flow and gas pressure. **h)** before and after optimization images of two lipid species from a tumor section.*

241 **Repeatability**

242 *Normalization*

243 Ion intensity variations will occur within ion images of a homogenous tissue surface, due to

244 slight variations in the spray conditions, tissue thickness/moisture content and conductivity of the

245 slide. The phenomenon is analogous with variations in matrix coverage/laser power in MALDI

246 imaging leading to similar fluctuation of signal intensity.[30] We calculated the CV of the signal

247 intensity of Rhodamine B, marked on a glass slide in the form of red ink. Over a 4 minute time

248 period the CV of the Rhodamine B was 11%. The mean CV of our tissue raw data (without

249 normalisation) was 55% (figure 3a), suggesting that tissue factors are responsible for a greater

250 contribution to this variation in signal intensity.

251 Normalization is justified to ensure that pixels are not excluded from a group based on

252 systematically lower ion intensities across all peaks within the spectrum. While fluctuation of

253 overall intensity can be corrected by normalization, it does not correct for missing peaks or other

254 pattern-level fluctuations in the spectra. Therefore, the pixels with different feature sets will be

255 separately classified by multivariate statistical analysis methods.

256 The aim of normalization is to account for variation in ion intensities that is complicit within the

257 acquisition and not a naturally occurring biological fluctuation over the surface of the sample. By

258 far the most commonly used method – in the field of imaging mass spectrometry – is to

259 normalize to the sum of all spectral intensities, otherwise known as the TIC. However, the

260 performance of this approach can be compromised by the unexpected intensity change of a single

261 high intensity peak.[31] Normalization to the base peak (unit vector normalization) is suitable when

262 the base peak is the same in each spectrum and it shows uniform intensity across the entire tissue

263 section (or histologically homogeneous segment).[32] However, even in cases where the tissue

264   section is assumed to be homogenous, this approach is still likely to fail due to undetermined

265   biological variation.
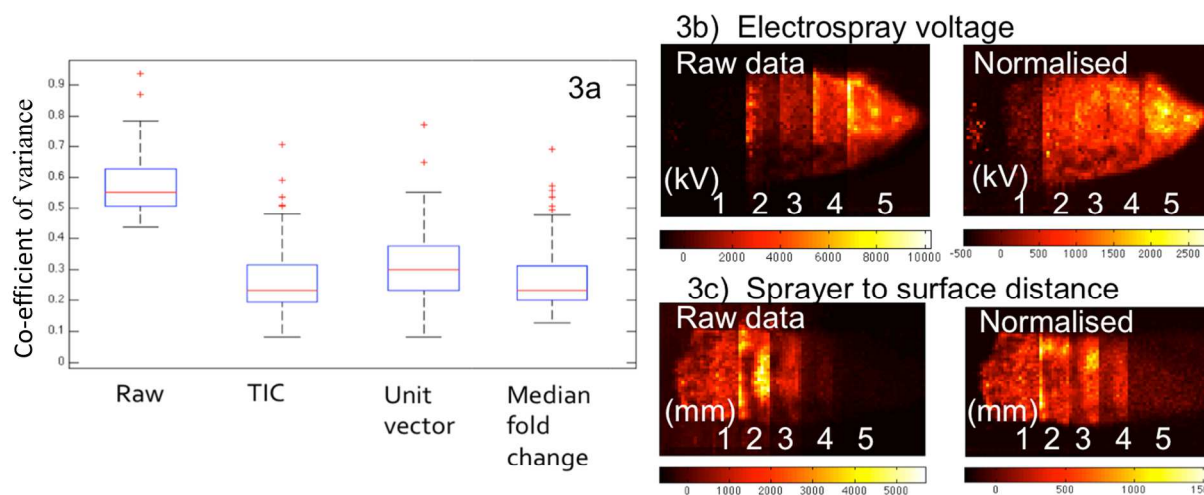
266
267   ***Figure 3 a)*** *Coefficient of variance for 65 lipid species identified in the 600-900 m/z range for*

268   *the full data set, and following different normalization methods.* ***b&c)*** *first principal component*

269   *score image of tissues analysed under varying conditions (electrospray voltage and sprayer to*

270   *surface distance respectively) when PCA analysis is performed on raw and then normalized*

271   *data.*

272   Although the spectra collected within the current study are expected to be highly uniform due to

273   the choice of tissue, the general purpose of tissue imaging experiments is still to identify regions

274   with different chemical profiles. Consequently, it would be desirable to have a normalization

275   technique that not only corrects for variance in the spectral intensity but also facilitates the

276   confident discovery of changes within lipid spectral patterns. For this reason we opt to use

277   median fold change within our workflow. From a computational point of view, the fold changes

278   of non-differentially expressed lipid species between pixels should be approximately one. If this

279   were not the case, the robust estimate of this systematic bias would be shown by the median of

280 fold changes of peak intensities of a given pixel with respect to the median profile across all

281 pixels.[33]

282 As seen in figure 3a, although the tissue samples are thought to be homogenous and all analysis

283 parameters were kept the same, the CV for the selected lipid species when all sixteen samples are

284 compared has a median value of 55% within the raw data, with some outliers in excess of 90%.

285 This is accounted for by day-to-day variation in the analysis as no single tissue section has a

286 median CV greater than 25%. All three of the normalization techniques discussed resulted in a

287 considerable improvement; however the outliers still remained, suggesting the presence of a

288 biological effect (heterogeneous distribution) as opposed to experimental.

289 Figure 3b and 3c illustrate the ability of normalization to correct for fluctuations in analysis

290 conditions. The image on the left shows the first principal component score image of the raw

291 data of tissue sections analysed under five varying conditions, electrospray voltage in 3b and

292 distance between sprayer tip and the tissue in 3c. The optimum setting is clearly demonstrated by

293 the raw data in both cases, with the other values having a lower contribution to the PC

294 proportionally to their distance from the optimum. When median fold normalization is carried

295 out, the PC1 scores demonstrate that the datasets acquired under different conditions now group

296 much closer together, although one would expect that these differences associated with

297 significant changes in experimental conditions cannot be eliminated by sole normalization.

298 However it is shown in 3c, the normalization can correct for a +/- 1mm change from the 2mm

299 optimum of the sprayer to tissue distance, far greater than any human error (precision of human

300 hands and eye). Similar observations were made for all of the conditions studied.

301

16

302   *Coefficient of variance of lipid species intra-section, intra-quadrant and inter-quadrant levels*

303   The CV of the 65 lipid species were calculated when each tissue section is analysed separately

304   (intra-section), when each tumor quadrant is treated as a single dataset (intra-quadrant) and

305   finally all sixteen sections combined into one dataset (inter-quadrant). The mean CV of the 65

306   lipid species (Supplementary file S3) was found to increase with each level of the hierarchy,

307   from intra-section (16±7%) to intra-quadrant (22±7%) to inter-quadrant (30±14%, figure 4a).

308   This is likely associated with increasing biological heterogeneity, which is a consequence of

309   increased distance separation between samples taken from the tumor. For example, the lipids

310   peaks with *m/z* value of 703.52 and 799.67 have a CV of 51% and 49% respectively, at the intra-

311   quadrant level. The high CV values of these single ions can be explained by biological

312   heterogeneity as shown by their non-uniform distribution across four tissue sections from the

313   first tumor quadrant (figure 4c). In comparison, the lipid peak m/z 790.56 has a more uniform

314   distribution across the four sections (figure 4b) and has a CV of only 7%. Despite the presence of

315   sample heterogeneity, many of the lipids demonstrate similar signal stability across the multiple

316   sections, especially the Phosphatidylethanolamine in the *m/z* range 720–760.

1
2
3
4
5
6
7
8
9
10
11
12
13
14
15
16
17
18
19
20
21
22
23
24
25
26
27
28
29
30
31
32
33
34
35
36
37
38
39
40
41
42
43
44
45
46
47
48
49
50
51
52
53
54
55
56
57
58
59
60
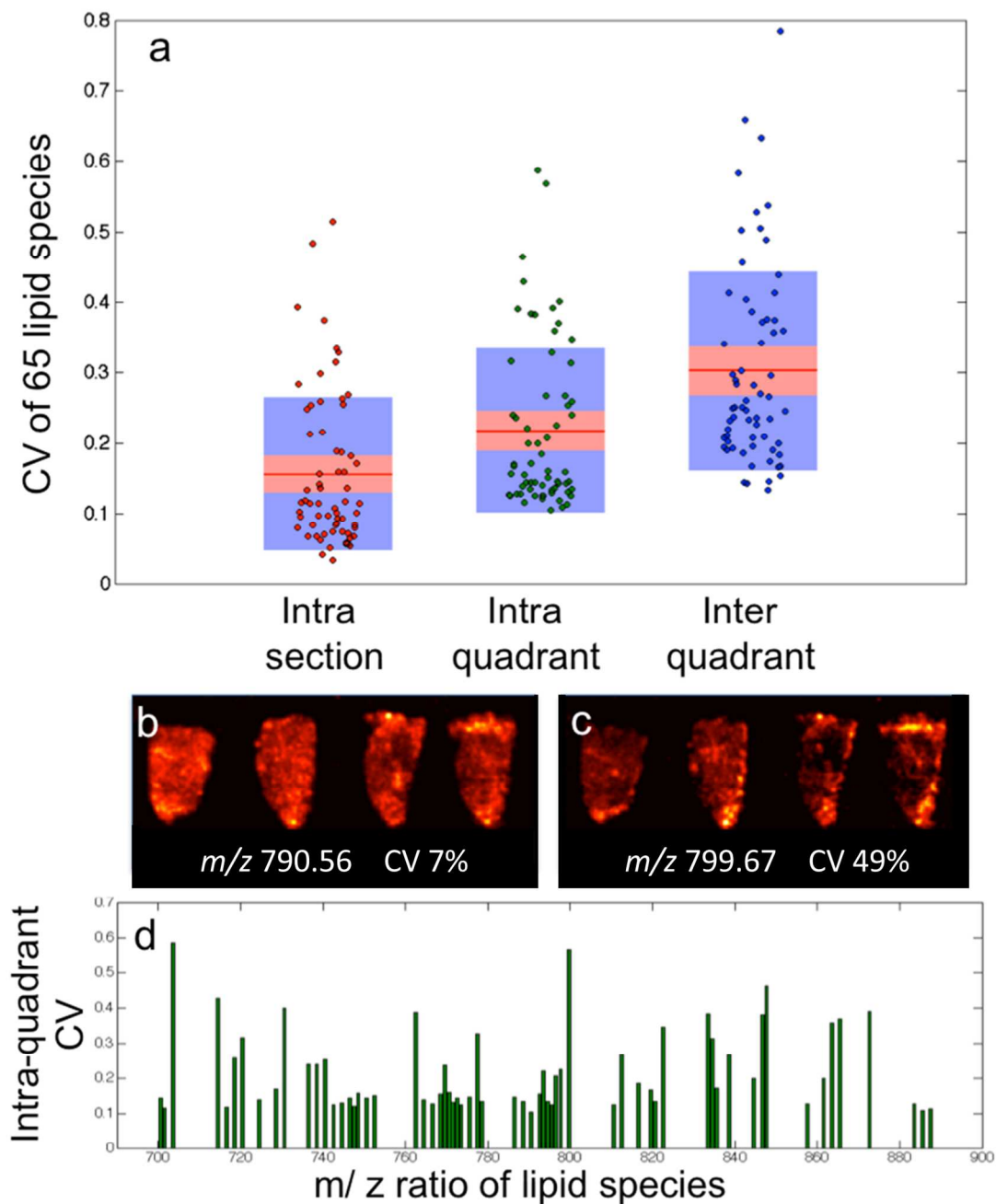
317

318 ***Figure 4 a)*** *Boxplot (mean, red band; 95% confidence, pink box; 1 standard of deviation, blue*
319 *box) representation for the coefficient of variance of 65 lipid species when each tissue section is*
320 *analysed separately (intra-section), when each tumor quadrant is treated as a single dataset*
321 *(intra-quadrant) and finally all sixteen sections combined into one dataset (inter-quadrant).* ***b)***
322 *Single ion (m/z=790.56) images of four sections from the same quadrant demonstrating*
323 *biological homogeneity with a low CV value* ***c)*** *Single ion (m/z=799.56) images of four sections*
324 *from the same quadrant demonstrating biological heterogeneity causing a high CV value.* ***d)***
325 *Intra-quadrant CV values for the 65 lipids plotted against mass to charge ratio to demonstrate*
326 *that there is no relationship with lipid mass.*

18

327   The intra-quadrant mean±SD CV of 22±7% is the best representation of the repeatability of the

328   instrument, as measurements are performed on different samples and have less contribution from

329   biological heterogeneity as found at the inter-quadrant level. The repeatability of the instrument

330   is such that if two regions of interest were compared from different samples, it would mean a

331   fold change of only 1.3 would be required to determine a significant difference with a 95%

332   confidence.

333   *Lipid profile pattern*

334   The variance of spectral pattern in a given histologically homogeneous region of a tissue is the

335   most critical parameter for multivariate statistics-based tissue classification workflows.

Figure 5 a) *Two colour overlays of m/z 885.6 (red) and m/z 863.6 (green) for all sixteen tissue sections used in the study (four replicates from each quadrants of the tumor). The m/z values of 885.6 and 863.6 represent the base peak in cancer tissue and abundant peak in stromal tissue, respectively. Inset, the first three principal component scores for twenty five randomly selected spectra from each section b) hierarchical cluster analysis of the mean spectral representation of four regions of interest from all sixteen sections.*

20

343 Consequently, the lipid profiles were compared by PCA, with the resulting score plot colour

344 coded by individual tissue section with each quadrant having its own colour group (figure 5a).

345 Loading plots are included in supplementary file S4. The data points in figure 5a from each

346 individual tissue section scatter within a single large group in the 3 dimensional PCA space (first

347 three components); with few outlying data points. Within the main cluster, it is evident that the

348 data groups from the different quadrants of the tumor show high levels of overlap. This is

349 expected as these sections are from spatially remote regions of the biological mass, whereas the

350 samples from the same quadrant are serial sections (original distance of corresponding voxels is

351 less than 50μm). The fact that there is no apparent sub-grouping within the individual quadrants

352 suggests that spectra from the same tissue analysed at different times cannot be differentiated

353 based on their lipid fingerprint. This is supported by the HCA in figure 5b where mean spectra

354 were created from four tumour specific areas from each section. Here again we see that each

355 quadrant clusters together, however, at the following level the sub-regions of each tissue section

356 do not cluster.

Reproducibility

358 The reproducibility of DESI-MS for the analysis of ion intensities of 25 selected lipid species is

359 demonstrated in figure 6. The mean CV±SD for the 25 lipid species from instrument 1 (Exactive

360 FTMS) and 2 (LTQ Orbitrap XL) were 10±5 and 16±7%, respectively. When data from the

361 DESI-MS platforms are combined, the reproducibility or mean CV±SD is 18±8%. In general, the

362 CVs of lipids for instrument 2 are greater than instrument 1, which can be attributed to a less

363 stable DESI-MS ion source and an inferior MS sensitivity. The CV for reproducibility is less

364 than that for repeatability as only sections from the fourth quadrant of the tumour were chosen

Analytical Methods Accepted Manuscript

21

365   for the purpose of analysis: to reduce the influence of biological heterogeneity confounding the

366   results (Supplementary file S3).

367
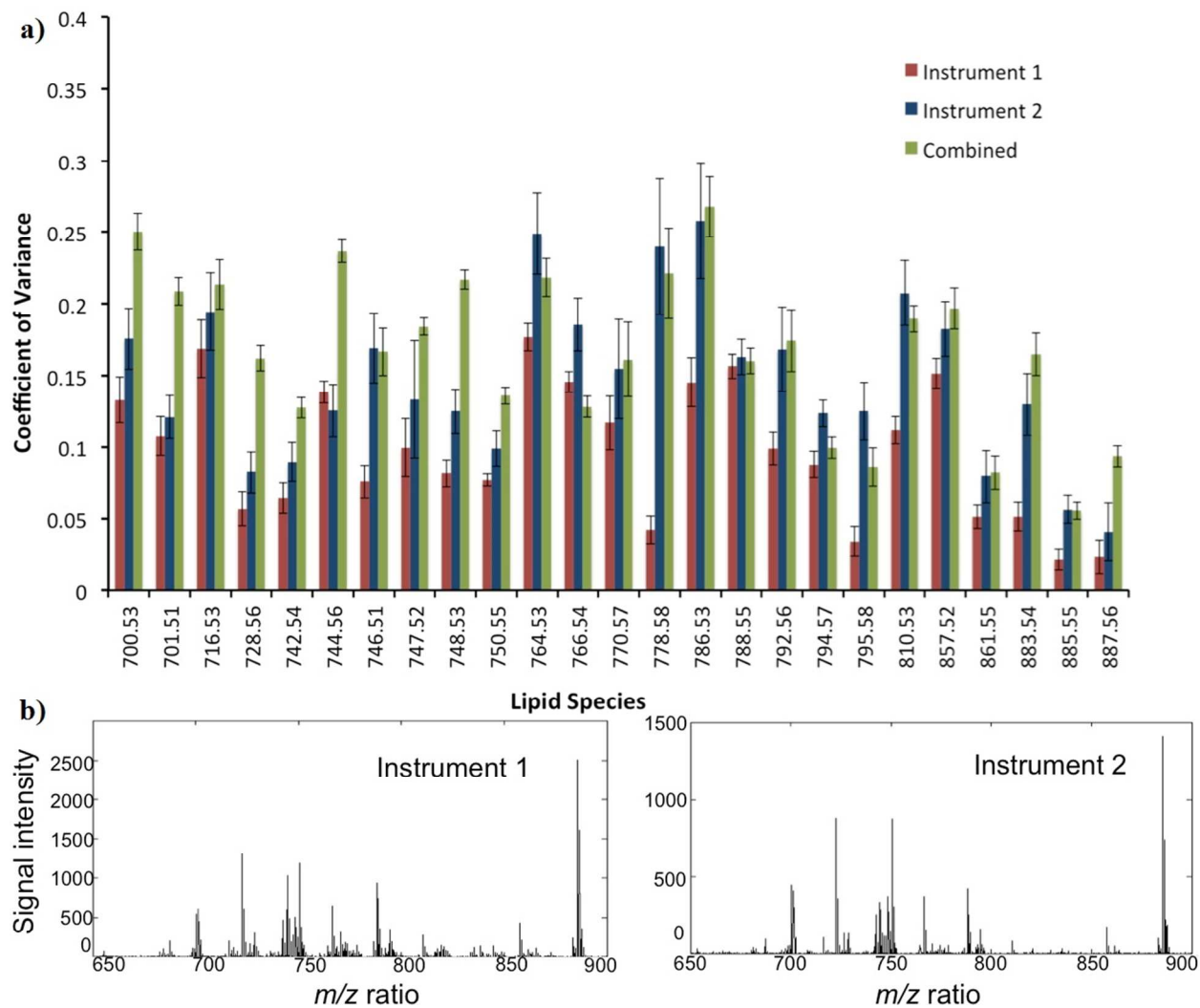
368

369   ***Figure 6 a)*** *Coefficient of variance for 25 lipid species from four sections of the same quadrant*
370   *when analysed on two different DESI-MS platforms and when the data is combined to determine*
371   *the reproducibility of the lipid profiles* ***b)*** *Representative mass spectra of lipid profiles from*
372   *instrument 1 (Exactive FTMS) and 2 (LTQ Orbitrap XL).*

373

374 In comparison, a study by Dill et al. investigated the reproducibility of DESI-MS in five serial

375 sections of rat brain.[34] The methodology, however, was more in keeping with repeatability rather

376 than reproducibility, which was assessed by two methods: first by calculating the ratio between

377 the absolute intensity of two main peaks and then performing an analysis of the full spectrum

378 based on normalized vectors. The best values for the ratio and normalized vector analysis were a

379 relative standard deviation (RSD) of 4.7%-8% and 0.8%, respectively.[34]

380 A study of human plasma lipid extracts with LC-MS demonstrated a CV of less than 15%.[35] A

381 further study of lipid extracts form rat heart/skeletal muscle mitochondria using HPLC-MS

382 showed an inter-day CV of ≤11% for different groups of glycerophospholipids.[36] However, these

383 studies did not adhere to the strict stipulated conditions for measuring reproducibility as per the

384 definition,[21] and therefore meaningful comparisons cannot be made with our data. In our study,

385 the results of reproducibility meet the requirements by the FDA, which states that the CV should

386 not exceed 20% as per chromatographic methods.[20]

387 **Conclusion**

388 This is the first study to report measurements of precision for the imaging analysis of human

389 cancer tissue using DESI-MS. The optimal parameters for the DESI-MS ion source were in

390 coarse agreement with the results of previous studies and they were consistent with the droplet

391 pick-up ionization mechanism of DESI-MS. Median fold change provided the optimal method

392 for normalization of data. Repeatability and reproducibility for measurements of lipid intensities

393 in tissue sections were 22% and 18%, respectively.

394 The reproducibility of DESI-MS is appropriate for accurate lipidomic profiling studies of human

395 tissue for meaningful inter-sample comparison of various disease states such as cancer. Due to

396　the inherent difficulties associated with introducing internal standards into intact human tissue,

397　the technique is limited to a semi-quantitative capacity which means that is better suited to lipid

398　ratio identification of specific tissue types, commonly referred to as the "fingerprint", which can

399　be used with increased confidence for the purpose of automated histology with MSI.

400　The evolving field of lipidomics will benefit from technologies that have an acceptable level of

401　precision for profiling and targeted studies of lipids in human disease. Well established

402　chromatographic techniques such as LC-MS have remained the gold standard due to their

403　quantitative capacity, range of lipid detection and ease of automation. However these techniques

404　generally build on lipid extraction-type sample preparation, which lack histological specificity,

405　encompassing all of the various cellular components rather than specific cells of interest. DESI-

406　MS not only has the added advantage of spatially and histologically resolved data acquisition, it

407　also has acceptable levels of reproducibility for the purposes of lipidomic profiling.

408　**Supporting Information**

409　Contents of material supplied as Supporting Information:

410　Supplementary files1: DESI Sprayer construction

411　Supplementary files 2: Home-built 3D XYZ integrated DESI-MS stage

412　Supplementary files 3: Mean CVs of 65 lipid peaks

413　Supplementary files 4: Loading plots

414

415　**Corresponding Author**

416　Zoltan Takats:

417　* Tel: (+) 44 (0)207 5942760. Email: z.takats@imperial.ac.uk

Author Contributions

419 ‡ NA and EJ are joint first authors and they contributed equally. The manuscript was written

420 through contributions of all authors. All authors have given approval to the final version of the

421 manuscript

Funding Sources

Acknowledgments

Abbreviations

430 DESI-MS, desorption electrospray mass spectrometry; MSI, Mass spectrometry imaging; total

431 ion count; MALDI, Matrix assisted laser desorption ionization; SIMS, secondary ion mass

432 spectrometry; MS, mass spectrometer; RSD, relative standard deviation; CV, co-efficient of

433 variance; ppm, parts per million; PCA, principal component analysis; HCA, hierarchical cluster

434 analysis ; SM, Sphingomyelin; PA, Phosphatidic acid; PS, Phosphatidylserine; HPLC-MS, high

435 performance liquid chromatography mass spectrometry; LC-MS, liquid chromatography mass

436 spectrometry.

437

438

439 **References**

440 1. S. M. Rahman, A. L. Gonzalez, M. Li, E. H. Seeley, L. J. Zimmerman, X. J. Zhang, M.

441 L. Manier, S. J. Olson, R. N. Shah, A. N. Miller, J. B. Putnam, Y. E. Miller, W. A.

442 Franklin, W. J. Blot, D. P. Carbone, Y. Shyr, R. M. Caprioli, and P. P. Massion, *Cancer*

443 *Res.*, 2011, **71**, 3009-17.

444

445 2. M. Shi, J. Jin, Y. Wang, R. P. Beyer, E. Kitsou, R. L. Albin, M. Gearing, C. Pan and J. J.

446 Zhang, *Neuropathol. Exp. Neurol.*, 2008, **67**, 117-24.

447

448 3. J. Pierson, J. L. Norris, H. R. Aerni, P. Svenningsson, R. M. Caprioli and P. E. Andren, *J.*

449 *Proteome Res.*, 2004, **3**, 289-95.

450

451 4. N. Zaima, T. Sasaki, H. Tanaka, X. W. Cheng, K. Onoue, T. Hayasaka, N. Goto-Inoue,

452 H. Enomoto, N. Unno, M. Kuzuya and M. Setou, *Atherosclerosis*, 2011, **217**, 427-32.

453

454 5. P. Fragu, J. Klijanienko, D. Gandia, S. Halpern and J. P. Armand, *Cancer Res.*, 1992, **52**,

455 974-7.

456

457 6. E. S. Lee, H. K. Shon, T. G. Lee, S. H. Kim and D. W. Moon, *Atherosclerosis*, 2013,

458 **226**, 378-84.

459

26

460   7.   A. N. Lazar, C. Bich, M. Panchal, N. Desbenoit, V. W. Petit, D. Touboul, L. Dauphinot,

461   C. Marquer, O. Laprevote, A. Brunelle and C. Duyckaerts, Acta. Neuropathol., 2013,

462   **125**, 133-44.

463

464   8.   N. E. Manicke, M. Nefliu, C. Wu, J. W. Woods, V. Reiser, R. C. Hendrickson and R. G.

465   Cooks, *Anal. Chem.*, 2009, **81**, 8702-7.

466

467   9.   S. Gerbig, O. Golf, J. Balog, J. Denes, Z. Baranyai, A. Zarand, E. Raso, J. Timar, Z.

468   Takats, *Anal. Bioanal. Chem.*, 2012, **403**, 2315-25.

469

470   10. L. S. Eberlin, I. Norton, A. L. Dill, A. J. Golby, K. L. Ligon, S. Santagata, R. G. Cooks

471   and N. Y. Agar, *Cancer Res.*, 2012, **72**, 645-54.

472

473   11. T. A. Masterson, A. L. Dill, L. S. Eberlin, M. Mattarozzi, L. Cheng, S. D. Beck, F.

474   Bianchi and R. G. Cooks, *J. Am. Soc. Mass. Spectrom.*, 2011, **22**, 1326-33.

475

476   12. E. Fahy, S. Subramaniam, H. A. Brown, C. K. Glass, A. H. Merrill Jr, R. C. Murphy, C.

477   R. Raetz, D.W. Russell, Y. Seyama, W. Shaw, T. Shimizu, F. Spencer, G. van Meer, M.

478   S. van Nieuwenhze, S. H. White, J. L. Witstum and E.A. Dennis, *J. Lipid Res.*, 2005, **46**,

479   839-61.

480
481

482   13. M. R. Wenk, *Nat. Rev.*, Drug Discov., 2005; **4**, 594-610.

483

484   14. Z. Takats, J. M. Wiseman and R. G. Cooks, *J. Mass. Spectrom.*, 2005, **40**, 1261-75.

485

486   15. K. A. Douglass, S. Jain, W. R. Brandt and A. R. Venter, *J. Am. Soc. Mass. Spectrom.*,

487   2012, **23**, 1896-902.

488

489   16. F. M. Green, P. Stokes, C. Hopley, M. P. Seah, I. S. Gilmore and G. O'Connor, *Anal.*

490   *Chem.*, 2009, **81**, 2286-93.

491

492   17. A. Venter, P. E. Sojka and R. G. Cooks, *Anal. Chem.*, 2006, **78**, 8549-55.

493

494   18. A. Badu-Tawiah, C. Bland, D. I. Campbell and R.G. Cooks, *J. Am. Soc. Mass. Spectrom.*,

495   2010, **21**, 572-9.

496

497   19. A. Bodzon-Kulakowska, A. Drabik, J. Ner, J. H. Kotlinska and P. Suder. *Rapid Commun.*

498   *Mass Spectrom.* 2014, **28**, 1-9.

499

500   20. U.S. Department of Health and Human Services Food and Drug Administration. Guidance

501   for industry: bioanalytical method validation. September 2013.

502   http://www.fda.gov/downloads/Drugs/GuidanceComplianceRegulatoryInformation/Guid

503   ances/UCM368107.pdf.

504

505   21. Analytical methods committee. AMC technical brief: Terminology - the key to

506   understanding analytical science. Part 1: Accuracy, precision and uncertainty, 2013.

507   Royal Society of Chemistry Web site.

508   http://www.rsc.org/lap/rsccom/amc/amc_index.htm. (accessed Nov 28, 2013)

509

510   22. M. Senko, S. Beu and F. McLafferty, *J. Am. Soc. Mass Spectrom.*, 1995, **6**, 52-56.

511

512   23. A. B. Costa and R. G. Graham, *Chem. Phys. Lett.*, 2008; **464**, 1-8.

513

514   24. A. Venter and R. G. Cooks, *Anal. Chem.*, 2007, **79**, 6398–6403.

515

516   25. H. Chen, N. N. Talaty, Z. Takáts and R. G. Cooks, *Anal. Chem.*, 2005, **77**, 6915–6927.

517

518   26. Z. Takats, S. C. Nanita, R. G. Cooks, G. Schlosser and K. Vekey, Anal. Chem., 2003; **75**,

519   1514.

520

521   27. R. Haddad, R. Sparrapan and M. N. Eberlin, *Rapid Commun. Mass Spectrom.*, 2006, **20**,

522   2901–2905.

523

524   28. H. Y. Liu and A. Montaser, *Anal. Chem.*, 1994, **66**, 3233.

525

526   29. A. Gomez and K. Q. Tang, *Physics of Fluids*, 1994, **6**, 404.

527

528   30. S-O. Deinenger, D. S. Cornett, R. Paape, M. Becker, C. Pineau, S. Rauser, A. Walch, E.

529   Wolski, *Anal. Bioanal. Chem.*, 2011, **401**, 167-181.

530

531   31. D. A. Cairns. D. Thompson, D. N. Perkins, A. J. Stanley, P. J. Selby, R. E. Banks,

532   *Proteomics*, 2008, **8**, 21-7.

533

534   32. G. T. Rasmussen and T. L. Isenhour, *J. Chem. Inf. Comput. Sci.,* 1979, **19**, 179–186.

535

536   33. K. A. Veselkov, L. K. Vingara, P. Masson, S. L. Robinette, E. Want, J. V. Li, R. H.

537   Barton, C. Boursier-Neyret, B. Walther, T. M. Ebbels, I. Pelczer, E. Holmes, J. C. Lindon

538   and J. K. Nicholson, *Anal. Chem.*, 2011, **83**, 5864-72.

539

540   34. A. L. Dill, L. S. Eberlin, A. B. Costa, D. R. Ifa and R. G. Cooks, *Anal. Bioanal. Chem.*,

541   2011, **401**, 1949-61

542
543

544   35. L. A. Heiskanen, M. Suoniemi, H. X. Ta, K. Tarasov and K. Ekroos, *Anal. Chem.*, 2013,

545   **85**, 8757-63.

546

547   36. J. Kim and C. L. Hoppel, *J. Chromatogr. B. Analyt. Technol. Biomed. Life Sci.*, 2013,

548   **912**, 105-14.